DOI: 10.31534/engmod.2025.1.ri.04d
Original scientific paper
Received: 7.05.2024.

Modelling and Analysis of Three-Dimensional Maxwell-Nanofluid Flow over a Bi-Directional Stretching Surface in the Presence of a Magnetic Field

Tanuku Poornakantha(1), **Mamidi Laksmiprsanna**(2), **Gundagani Murali**(3)

(1) *Department of Mathematics, GVP College of Engineering for Women, Visakhapatnam, INDIA*

(2) *Department of Mathematics, Andhra University, INDIA*

(3) *Department of Mathematics, Geethanjali College of Engineering and Technology, Cheeryal, INDIA*
e-mail: murali.maths81@gmail.com

SUMMARY

This work models a three-dimensional, steady, incompressible, viscous, non-Newtonian Maxwell fluid flow over a bidirectional stretching surface, both computationally and numerically. Under Brownian motion, thermophoresis, thermal, and mass Biot numbers, the effects of Soret and Dufour on three-dimensional upper-convected Maxwell-Nanofluid flow across a bidirectional stretching surface are examined in the current study. The latest information on the unique and innovative properties of nanofluids is also provided. The energy equation includes a nonlinear radiative heat flow, according to the Rosseland approximation. By adding applicable dimensionless variables and parameters, the governing equations are converted to dimensionless form and solved via a finite element system. The study provides a thorough examination of the ways different variables and other relevant parameters affect the flow variables. These findings are made visually clear and offer valuable insight into the flow scenario using graphical representations. The results indicate that the plan is appropriate for solving the current issue. This new research has implications for energy systems, biomedical engineering, and aeronautics, as well as significant implications for the food industry. This investigation's numerical findings are felt and validated.

KEY WORDS: *Maxwell-nanofluid; finite element method; magnetic field; three-dimensional; thermal Biot number; mass Biot number.*

1. INTRODUCTION

It is critical to include radiative heat flow while studying heat transfer processes, especially with nanofluids. Radiative heat transfer is made using electromagnetic waves throughout the energy transmission process. Heat transmission properties can be adjusted further with the presence

of nanofluids, which are liquid suspensions containing microscopic particles. The Stefan-Boltzmann equation and other linear models that presuppose a linear relationship between the temperature difference and radiative heat flow have historically been used to characterize radiative heat transfer. When attempting to accurately depict the behaviour of heat transfer, a non-linear radiative heat flow model might be more suitable. To counteract the radiative characteristics of the nanofluid, such as the radiation absorption and scattering by the floating nanoparticles, a non-linear radiative heat flow is added. The fluid's effective thermal conductivity, absorption, and emission characteristics can all be changed by these factors, which can then affect radiative heat transfer. The non-linear radiative heat flow in the presence of a nanofluid can be described in a variety of ways. Nanoparticle concentration, size, and shape are often considered while estimating radiative heat transfer, using complex models that account for the interactions. The extinction coefficient and scattering phase function of the nanofluid, as well as other radiative properties, may be determined through experiments. In order to make more accurate forecasts, these observable characteristics can then be included in non-linear radiative heat transfer models. A fluid is a unique type of matter with the capacity to flow and undergo effortless distortion when an external force is applied. Non-Newtonian fluids have innumerable real-life applications in natural products, biomedical fields, agriculture, and food products. Exhaustive benefits in various fields have made budding researchers study and investigate the attributes of non-Newtonian fluids. Over the past decade, the non-Newtonian liquid stream has gained significant attention due to its diverse applications in engineering and industrial sectors. The Maxwell liquid model is a crucial rate-type fluid subclass, and recent studies have focused on modelling and exploring nanoliquid streams. Nanoparticles are used to increase heat transmission and overcome cooling issues in thermal frames. Researchers have studied nanoliquid streams as they pass through surfaces, as simple Navier-Stokes equations cannot represent some fluids due to their complicated rheology.

The radiative heat transport characteristics of nanofluids were studied in [1]. A comprehensive analysis of magnetohydrodynamic (MHD) Maxwell fluid flow incorporating nanoparticles over a stretching surface was conducted in [2], considering the effects of thermal radiation, convective boundary conditions, and an induced magnetic field. The thermal and diffusion influences on MHD Jeffrey fluid flow over a porous stretching sheet were explored in [3], factoring in activation energy. A model to analyze MHD micropolar nanofluid flow over a Darcian porous stretching surface was developed in [4], addressing thermophoretic and Brownian diffusion phenomena. A perturbative study on radiation absorption, Hall effect, and ion-slip current-driven MHD convection was performed in [5], focusing on spanwise cosinusoidally fluctuating temperature profiles. The role of a quadratic-linearly radiating heat source in conjunction with Carreau nanofluid and exponential space dependency was examined in [6], particularly in applications related to cones and wedges, with relevance to medical engineering and renewable energy contexts. Bio-convection phenomena involving slippery two-phase Maxwell nanofluid flow past a vertically induced magnetic stretching regime were investigated in [7], with implications for biotechnology and engineering. Insights into the flow dynamics of nanofluids were presented in [8], modelling various fluid flow challenges. A response surface methodology (RSM) analysis on slip effects in Casson nanofluid flow over a stretching sheet with activation energy considerations was conducted in [9]. A numerical study on magneto-hydro-convective nanofluid flow within a porous square enclosure was performed in [10]. The impact of nanofluids and porous structures on the thermal efficiency of wavy channel heat exchangers was investigated in [11]. Analytical solution of forced convective heat transfer in tubes partially filled with metallic foam using the two-equation model was found [12]. Articles [13-23] highlight

potential applications. References [24-32] used the finite element method to address heat and mass transport in MHD flows effectively. Studies in [33-37] explored heat and mass transfer effects, significantly enhancing the understanding of the reported work.

When the magnetic field and non-radiative heat flux are present, relatively few studies have documented the three-dimensional analysis of nanofluid flow, according to a review of the works described above. There haven't yet been any reports in the literature on the combined effects of Soret and Dufour on steady, three-dimensional, incompressible, viscous, electrically conducting non-Newtonian upper convected Maxwell-Nanofluid flow over a bi-directional stretching sheet (surface) in the presence of non-linear radiative heat flux, Brownian motion, thermophoresis, thermal, and mass Biot numbers. This model is an enhanced version of previously published research. The outcomes of the current numerical simulations are also distinct.

2. MATHEMATICAL FORMULATION

This section covers the effects on 3-D, steady, incompressible, viscous, non-Newtonian Maxwell fluid flow over a bidirectional stretching surface of thermophoresis, Brownian motion, Soret, and Dufour. Figure 1 depicts the fluid flow's shape.

In this study, the following premises are assumed:

i. The sheet moves with velocities of U_w (x) = ax and V_w (y) = by in the x and y axes, respectively.
ii. The flow is subjected to a magnetic field with the strength of Bo in this study.
iii. The energy equation neglects the effects of ohmic heating, viscous dissipation, heat source, and Joule heating, and it assumes the effects of thermophoresis, Brownian motion, and Dufour.
iv. The species concentration equation considers the effect of thermal diffusion and neglects the chemical reaction effect.
v. T_w signifies the constant temperature and T_∞, the temperature of the fluid outside the thermal boundary layer.
vi. The convective boundary condition is applied when a hot fluid with a uniform temperature Tf, concentration φf, convective heat transfer coefficient $\beta 1$, and mass transfer coefficient $\beta 2$ heats the surface of a sheet.
vii. The magnetic Reynolds number is the minimum possible to neglect the generated magnetic field.

The equation for continuity:

$$\frac{\partial u}{\partial x}+\frac{\partial v}{\partial y}+\frac{\partial w}{\partial z}=0 \tag{1}$$

Momentum Equation:

$$u\left(\frac{\partial u}{\partial x}\right)+v\left(\frac{\partial u}{\partial y}\right)+w\left(\frac{\partial u}{\partial z}\right)+\lambda\left\{\begin{matrix} u^2\left(\frac{\partial^2 u}{\partial x^2}\right)+v^2\left(\frac{\partial^2 u}{\partial y^2}\right)+w^2\left(\frac{\partial^2 u}{\partial z^2}\right)+ \\ 2uv\left(\frac{\partial^2 u}{\partial x\partial y}\right)+2vw\left(\frac{\partial^2 u}{\partial y\partial z}\right)+2uw\left(\frac{\partial^2 u}{\partial x\partial z}\right) \end{matrix}\right\}=\frac{\partial^2 u}{\partial z^2}-\left(\frac{\sigma B_o^2}{\rho}\right)u \tag{2}$$

$$u\left(\frac{\partial v}{\partial x}\right)+v\left(\frac{\partial v}{\partial y}\right)+w\left(\frac{\partial v}{\partial z}\right)+\lambda\left\{\begin{matrix}u^2\left(\frac{\partial^2 v}{\partial x^2}\right)+v^2\left(\frac{\partial^2 v}{\partial y^2}\right)+w^2\left(\frac{\partial^2 v}{\partial z^2}\right)+\\ 2uv\left(\frac{\partial^2 v}{\partial x\partial y}\right)+2vw\left(\frac{\partial^2 v}{\partial y\partial z}\right)+2uw\left(\frac{\partial^2 v}{\partial x\partial z}\right)\end{matrix}\right\}=\frac{\partial^2 v}{\partial z^2}-\left(\frac{\sigma B_o^2}{\rho}\right)v \tag{3}$$

Thermal energy Equation:

$$u\left(\frac{\partial T}{\partial x}\right)+v\left(\frac{\partial T}{\partial y}\right)+w\left(\frac{\partial T}{\partial z}\right)=\alpha\left(\frac{\partial^2 T}{\partial z^2}\right)+\left(\frac{(\rho C)_p}{(\rho C)_f}\right)\left\{D_B\left(\frac{\partial T}{\partial z}\right)\left(\frac{\partial \varphi}{\partial z}\right)+\frac{D_T}{T_\infty}\left(\frac{\partial T}{\partial z}\right)^2\right\}$$
$$-\frac{1}{\rho C_p}\left(\frac{\partial q_r}{\partial z}\right)+\frac{D_m K_T}{C_s C_p}\left(\frac{\partial^2 \varphi}{\partial z^2}\right) \tag{4}$$

Species Concentration Equation:

$$u\left(\frac{\partial \varphi}{\partial x}\right)+v\left(\frac{\partial \varphi}{\partial y}\right)+w\left(\frac{\partial \varphi}{\partial z}\right)=D_B\left(\frac{\partial^2 \varphi}{\partial z^2}\right)+\frac{D_T}{T_\infty}\left(\frac{\partial T}{\partial z}\right)^2+\frac{D_m K_T}{T_m}\left(\frac{\partial^2 T}{\partial y^2}\right) \tag{5}$$

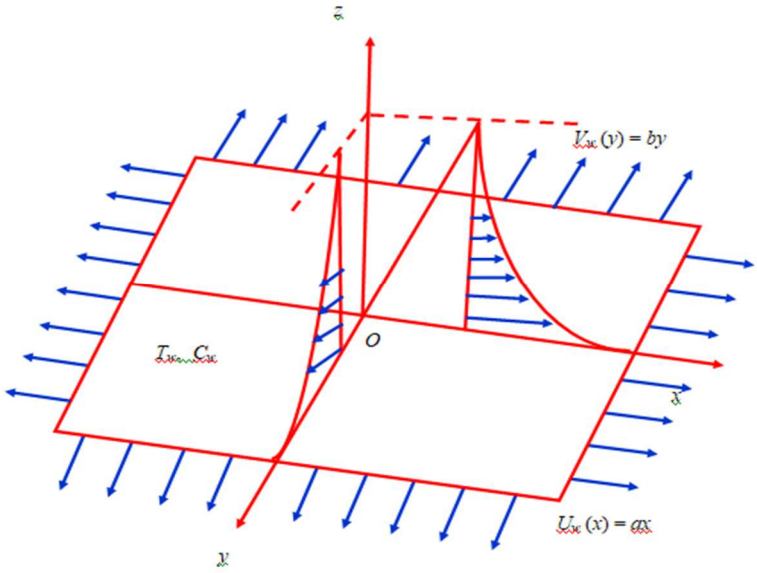

Fig. 1 *Nano-Maxwell fluid flow graphical representation*

The following are flow boundary conditions:

$$\left.\begin{matrix}u=U_w=ax,\ v=V_w=by,\ w=0,\ -\kappa\frac{\partial T}{\partial z}=\beta_1\left(T_f-T\right),\ -D_B\frac{\partial C}{\partial z}=\beta_2\left(\varphi_f-\varphi\right)\ at\ z=0\\ u\to 0,\ v\to 0,\ T\to T_\infty,\ \varphi\to\varphi_\infty\ as\ z\to\infty\end{matrix}\right\} \tag{6}$$

With the Roseland approximation, the radiative heat flux is defined as:

$$\frac{\partial q}{\partial r}=-\frac{1.3\sigma^*}{K^*}T_z \tag{7}$$

$$T^4=T_\infty^4+4T_\infty^3\left(T-T_\infty\right)+6T_\infty^2\left(T-T_\infty\right)^2+..... \tag{8}$$

After disregarding higher-order terms after the first degree term $(T-T_\infty)$, we get:

$$T^4 \cong 4T_\infty^3 T - 3T_\infty^4 \tag{9}$$

From (7) and (9), we get:

$$q_r = -\frac{5.3T_\infty^3\sigma^*}{K^*}T_z \tag{10}$$

(8) allows Eq. (3) to be expressed as:

$$uT_x + vT_y + wT_z = \alpha T_{zz} + \left(\frac{(\rho C)_p}{(\rho C)_f}\right)\left(D_B T_z C_z + \frac{D_T}{T_\infty}(T_z)^2\right) + \frac{1}{\rho C_p}T_{zz}\left(\frac{16T^3\sigma_\infty^*}{3\kappa k^*}\right) + \frac{D_m K_T}{C_p C_s}C_{zz} \tag{11}$$

Initiating the following similarity transformations:

$$\left.\eta = \left(\sqrt{\frac{a}{\nu}}\right)z,\ u = axf'(\eta), v = ayg'(\eta),\ \theta = \frac{T-T_\infty}{T_f-T_\infty},\ \varphi = \frac{\varphi-\varphi_\infty}{\varphi_f-\varphi_\infty}, w = \nu\sqrt{\nu a}\{f(\eta)+g(\eta)\},\ \right\} \tag{12}$$

Via 12 Eqs. (2), (3), (4), and (11) take the following form:

$$f'''-f'^2+ff''+gf''-Mf'+K\left\{2ff'f''+2gf'f''-(f+g)^2f'''\right\}=0$$

$$g'''-g'^2+fg''+gg''-Mg'+K\left\{2fg'g''+2gg'g''-(f+g)^2g'''\right\}=0$$

$$(f\theta')Pr+Prg\theta'+(NbPr)\phi'+PrNt(\theta')^2+(DuPr)\phi''+\left\{\frac{d}{d\eta}\left[1+R\left[1+(\theta_w-1)\theta\right]^3\theta'\right]\right\}$$

$$Nb\phi''+NbScf\phi'+NbScg\phi'+Nt\theta''+ScNbSr\theta''=0$$

The associated boundary conditions (6) become:

$$\left.\begin{aligned} &f(0)=0,\ g(0)=0,\ f'(0)=1,\ g'(0)=C,\ \theta'(0)=-\delta(1-\theta(0)),\ \phi'(0)=-\zeta(1-\phi(0)),\\ &f'(\infty)\to 0, g'(\infty)\to 0, \theta(\infty)\to 0,\ \phi(\infty)\to 0 \end{aligned}\right\}$$

If the relevant physical parameters are described as:

$$\left.\begin{aligned} &M=\frac{\sigma B_o^2}{\rho U_o}, K=\lambda_1 a,\ C=\frac{b}{a},\ \theta_w=\frac{T_w}{T_\infty}, Nb=\frac{\tau_B D_B(\varphi_f-\varphi_\infty)}{\nu}, Pr=\frac{\nu}{\alpha}, \delta=\frac{\beta_1}{\kappa}\sqrt{\frac{\nu}{a}}, \zeta=\frac{\beta_2}{D_B}\sqrt{\frac{\nu}{a}},\\ &Nt=\frac{\tau_B D_T(T_f-T_\infty)}{\nu T_\infty}, Sr=\frac{D_m K_T(T_f-T_\infty)}{T_m\nu(\varphi_f-C_\infty)}, Du=\frac{D_m K_T(\varphi_f-\varphi_\infty)}{C_s C_p\nu(T_f-T_\infty)}, Sc=\frac{\nu}{D_B},\ R=\frac{16\sigma^* T_\infty^3}{3\kappa k^*} \end{aligned}\right\} \tag{13}$$

Quantities of physical interest, the physical parameters, are presented as follows:

$$C_{fx}=\frac{\tau_{wx}}{\rho U_w^2}=\frac{1}{\rho U_w^2}\mu\left(\frac{\partial u}{\partial y}\right)_{y=0} \Rightarrow Cfx = C_{fx}\left(\sqrt{Re_x}\right)=f''(0) \tag{14}$$

$$C_{fy}=\frac{\tau_{wy}}{\rho V_w^2}=\frac{\mu}{\rho V_w^2}\left(\frac{\partial v}{\partial y}\right)_{y=0} \Rightarrow Cfy = C_{fy}\left(\sqrt{Re_y}\right)=g''(0) \tag{15}$$

$$Nu=-\left(1+R\theta_w^3\right)\left(\sqrt{Re_x}\right)\theta'(0) \tag{16}$$

$$Sh = \frac{xq_m}{D_B\left(C_f - C_\infty\right)} = -\frac{x\left(\frac{\partial C}{\partial y}\right)_{y=0}}{D_B\left(C_f - C_\infty\right)} \Rightarrow Sh = -\left(\sqrt{Re_x}\right)\varphi'(0) \tag{17}$$

$$Re_x = \frac{u_x(x)x}{\nu} \tag{18}$$

$$Re_y = \frac{v_w(y)y}{\nu} \tag{19}$$

Based on the stretching velocities above, local Reynolds numbers (18) and (19) have been shown.

3. SOLUTION OF THE MATHEMATICAL PROBLEM USING THE FINITE ELEMENT METHOD

This study employs the finite element method, a powerful technique for solving linear and nonlinear partial and ordinary differential equations prevalent in physics and mechanical engineering. Its utility extends to future research endeavours. A primary application of this method involves solving constructed equations, where the accurate approximation of real functions using form functions is crucial when dealing with real numbers. Rigorous adherence to this methodology ensures computational precision. The steps involved in FEM are shown in Figure 2.

The inflow sphere model comprises 10,000 identical quadratic factors, resulting in 20,001 nodes. Each factor possesses a uniform shape and magnitude, mirroring its counterparts. Following the formulation of element equations, 80,004 nonlinear equations remained for analysis. Subsequently, these equations were processed. Gaussian elimination, a well-established technique, was applied to resolve the equations, incorporating boundary conditions. This method yielded a solution with accuracy within 1/100,000 degrees. Gaussian quadrature facilitated the necessary integration simplifications. The computational implementation was achieved using the Mathematica programming language.

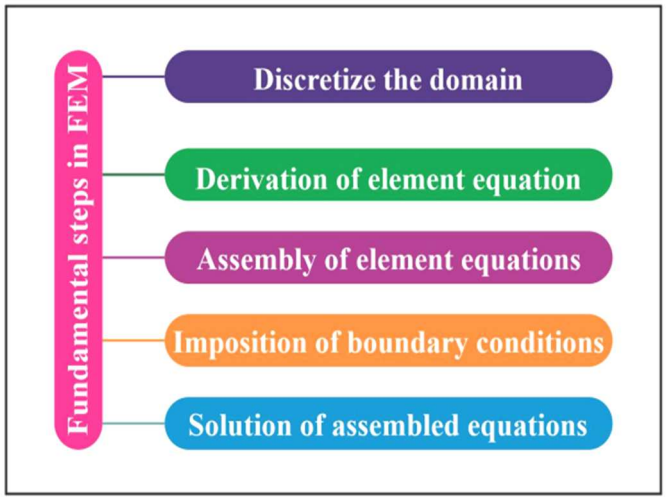

Fig. 2 *Fundamental steps in FEM*

Program Code Validation

Table 1 *Comparison between the current numerical results and the published results for various values of C from Ammar Mushtaq et al. [38] at Pr = 1.0 when M = 0, Nb = 0, Nt = 0, Sr = 0, Du = 0, ζ → ∞ and δ → ∞*

C	*Present numerical results*			*Results of Ammar Mushtaq et al. [38]*		
	$-f''(0)$	$-g''(0)$	$-\theta'(0)$	$-f''(0)$	$-g''(0)$	$-\theta'(0)$
0.25	1.0385679834	0.1867437347	0.6545640347	1.048811	0.194564	0.665926
0.50	1.0826347693	0.4560274634	0.7210683909	1.093095	0.465205	0.735333
0.75	1.1286789826	0.7826707660	0.7820676830	1.134486	0.794618	0.796472
1.00	1.1668398949	1.1668398949	0.8425687981	1.173721	1.173721	0.851992

Table 2 *Comparison of present numerical results with the published results of Liu and Anderson [39] for different values of C at Pr = 1.0 when M = 0, K = 0, R = 0, Nb = 0, Nt = 0, Sr = 0, Du = 0, ζ → ∞ and δ → ∞*

C	*Present numerical results*			*Results of Liu and Anderson [39]*		
	$-f''(0)$	$-g''(0)$	$-\theta'(0)$	$-f''(0)$	$-g''(0)$	$-\theta'(0)$
0.25	1.0286896981	0.1850897908	0.6477834499	1.048813	0.194565	0.665933
0.50	1.0798579345	0.4487475729	0.7188967643	1.093096	0.465206	0.735334
0.75	1.1183468884	0.7798774410	0.7776784938	1.134486	0.794619	0.796472

Tables 1 and 2 compare the authors' most recent numerical findings for various values of C at Pr = 1.0 with those previously reported by Ammar Mushtaq et al. [38] and Liu and Anderson [39]. The aforementioned findings show how closely our numerical results agree with the results of the previous research.

4. RESULTS AND DISCUSSION

The authors solved the governing flow ordinary differential equations (8), (9), (10), and (11) using the finite element method and boundary equations (12). In this part, the authors use several figures to demonstrate how various factors might affect equations for temperature, concentration, and dimensionless velocity (velocity components along the x and y axes). The parameter ranges for the graphical representations are built on the following critical values: M (Magnetic field parameter) = 0.5, K (Maxwell fluid parameter or Deborah number) = 0.5, C (Velocity ratio parameter) = 0.5, Pr (Prandtl number) = 0.22, R (Thermal radiation parameter) = 0.5, Nb (Brownian motion parameter) = 0.5, Nt (Thermophoresis parameter) = 0.5, Du (Dufour number) = 0.5, Sr (Soret number) = 0.5, Sc (Schmidt number) = 0.22, δ (Thermal Biot number) = 0.1, ζ (Mass Biot number) = 0.1, and θ_w (Temperature ratio parameter) = 0.5 (see 3 – Figure 20).

Figures 3 and 4 are affected by the Magnetic field parameter (M) on velocity profiles along the x - and the y – directions, respectively. The velocity fields are shown to diminish as the value of M rises. The fluid flow tends to slow down in the presence of a magnetic field, which reduces the thickness of the velocity and momentum boundary layers. The influence of the Maxwell fluid parameter or Deborah number (K) on the x - and y - components of velocity is sketched in Figures 5 and 6, respectively. The deviation of the fluid relaxation period from its basic time scale is quantified by the Deborah number. The relaxation period is the amount of time that fluid requires to reach equilibrium following the application of the shear force. It is anticipated that fluids with higher viscosity may take longer to relax. It is possible to interpret an increase in K in this way because fluid viscosity restricts fluid motion and lowers velocity. As a result, the

hydrodynamic boundary layer thins when K is increased. It is also noted that the change in the velocity fields f' and g' is larger in the three-dimensional flow when compared with the two-dimensional and axi-symmetric flows.

Figures 7 and 8 show the behavior of the velocity ratio parameter (C) on primary and secondary velocity profiles, respectively. From these figures, it is observed that both the primary and secondary velocity profiles are increasing with rising values of the velocity ratio parameter. The variation of the Prandtl number on temperature outlines is shown in Figure 9. It is concluded that increasing values of the Prandtl number result in a thinner temperature boundary layer thickness. Fluids with larger Prandtl numbers have lower thermal diffusivity, and hence the temperature decreases. Figure 10 shows the variations in temperature profiles due to an increase in the values of (R). Because the conduction effect of the nanofluid increases in the presence of R, it is noticed that the fluid temperature rises as R increases. Higher values of R thus imply higher surface heat flow, which raises the temperature in the boundary layer area.

The influence of the Brownian motion parameter (Nb) on temperature and concentration profiles is depicted through Figure 11 and Figure 12, respectively. These graphs show that when the values of the Brownian motion parameter increase, the thickness of the thermal boundary layer grows and the temperature differential at the surface decreases. When the Brownian motion parameter is raised, however, the concentration profiles and concentration boundary layer thickness show the reverse trend. Figs. 13 and 14 serve to demonstrate the impact of the thermophoresis parameter (Nt) on temperature and concentration curves. The findings demonstrate that the temperature and concentration boundary layer thickness rise as the thermophoresis parameter grows. By contrasting Figures 15 and 16 one after the other, you can see how the Dufour number (Du) and the Soret number (Sr) change in relation to the temperature and concentration profiles. Looking at this graph, we can see that increasing *Du's* value led to a rise in the temperature and thickness of the thermal layer. Physically, Du has to do with how a concentration gradient affects the thermal energy of a liquid. Growing Sr values also enhance concentration profiles, much like growing Sr levels do. This is because when there is a temperature gradient, the mass may move more readily from a location of lower to higher solute concentration. How the Schmidt number (Sc) impacts the concentration profiles is seen in Figure 17. The Sc value is a representation of the mass diffusivity to momentum ratio. It is possible to evaluate the relative importance of momentum and mass transfer using diffusion in the concentration (species) boundary layer. Lower concentration profiles will arise from a decrease in the fluid's mass diffusivity brought on by higher Sc. Due to the inverse relationship between mass diffusivity and Sc, weaker concentration boundary layers are linked to higher Sc concentrations. The temperature field's impact on the thermal Biot number (δ) is shown in Figure 18. With an increase, convection intensifies, raising the temperature field.

Figure 19 illustrates the effect of the mass Biot number (ζ) on the concentration profiles. Concentration profiles are an increasing function of the mass Biot number. Figure 20 includes the behavior of the temperature ratio parameter θ_w on the temperature distribution. Higher values of θ_w correspond to a higher temperature and thicker thermal boundary layer. This is explained as follows. It is clear from energy Eq. (10) that effective thermal diffusivity is the sum of classical thermal diffusivity (α) and thermal diffusivity due to the radiation effect. Thus, one anticipates that parameter θ_w, being the coefficient of the later term, would support the thermal boundary layer thickness. It can be noticed that the profiles attain a special S-shaped form when θ_w enlarges, which dictates the existence of an adiabatic case. In other words, the wall temperature gradient approaches zero value when the wall-to-ambient temperature ratio is sufficiently large.

The numerical values of various parameters, namely, M (magnetic field parameter), K (Maxwell fluid parameter or Deborah number), C (velocity ratio parameter), Pr (Prandtl number), R (thermal radiation parameter), Nb (Brownian motion parameter), Nt (thermophoresis parameter), Du (Dufour number), Sr (Soret number), Sc (Schmidt number), δ (thermal Biot number), ζ (mass Biot number), and θ_w (temperature ratio parameter) on skin-friction coefficients along the x - (Cfx) and y - (Cfy) directions are discussed in tables 3 and 4, respectively. From these tables, it is observed that the skin-friction coefficients along the x - (Cfx) and y - (Cfy) directions increase with increasing values of C (velocity ratio parameter), R (thermal radiation parameter), Nb (Brownian motion parameter), Nt (thermophoresis parameter), Du (Dufour number), Sr (Soret number), δ (thermal Biot number), ζ (mass Biot number), and θ_w (temperature ratio parameter) and decrease with increasing values of M (magnetic field parameter), K (Maxwell fluid parameter or Deborah number), Pr (Prandtl number), and Sc (Schmidt number). The tabular values of the rate of heat transfer coefficient or Nusselt number (Nu_x) for different values of Pr (Prandtl number), R (thermal radiation parameter), Nb (Brownian motion parameter), Nt (thermophoresis parameter), Du (Dufour number), δ (thermal Biot number), and θ_w (temperature ratio parameter) are shown in Table 5. From this table, it is observed that the rate of heat transfer coefficient increases with rising values of R (thermal radiation parameter), Nb (Brownian motion parameter), Nt (thermophoresis parameter), Du (Dufour number), δ (thermal Biot number), and θ_w (temperature ratio parameter), and the opposite effect is observed with the effect of Prandtl number (Pr). The effects of Nb (Brownian motion parameter), Nt (thermophoresis parameter), Sr (Soret number), Sc (Schmidt number), and ζ (mass Biot number) on the rate of mass transfer coefficient or Sherwood number (Sh_x) are studied through tabular forms in Table 6. From this table, it is observed that the rate of mass transfer coefficient increases with rising values of Nt (thermophoresis parameter), Sr (Soret number), and ζ (mass Biot number) and decreases with increasing values of Nb (Brownian motion parameter), and Sc (Schmidt number).

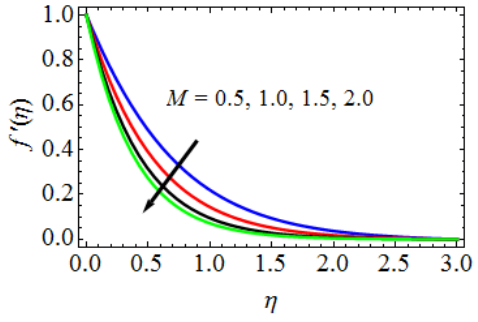

Fig. 2 *Velocity profiles along x - direction for different values of M*

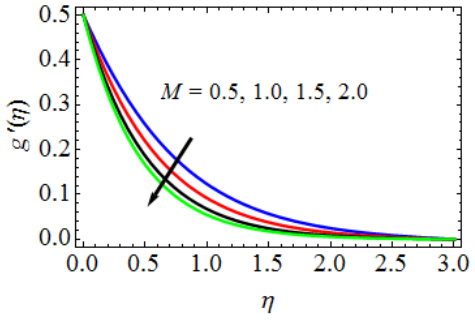

Fig. 3 *Velocity profiles along y - direction for different values of M*

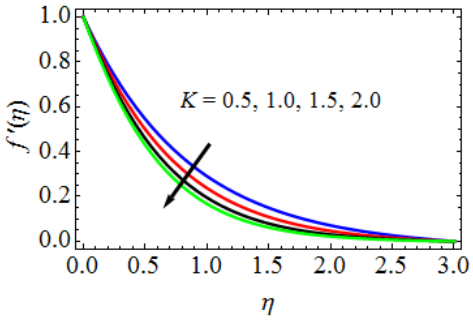

Fig. 4 *Velocity profiles along x - direction for different values of K*

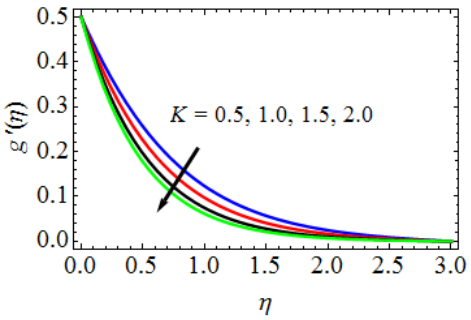

Fig. 5 *Velocity profiles along y - direction for different values of K*

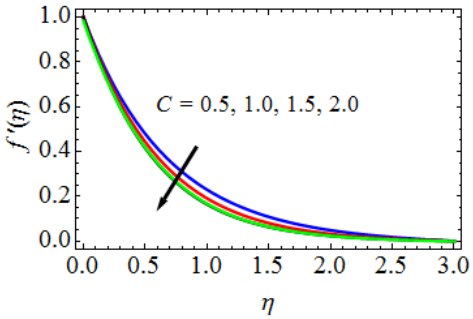

Fig. 6 *Velocity profiles along x - direction for different values of C*

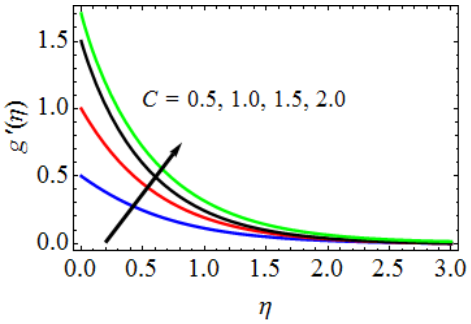

Fig. 7 *Velocity profiles along y - direction for different values of K*

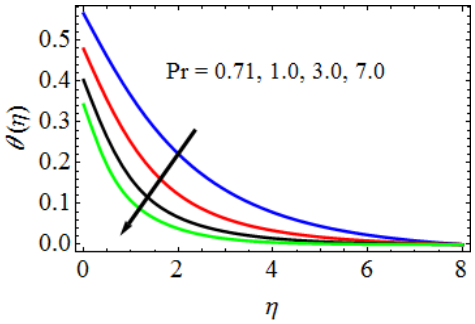

Fig. 8 *Temperature for different values of Pr*

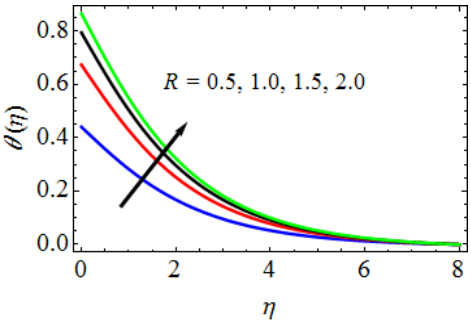

Fig. 9 *Temperature profiles for different values of R*

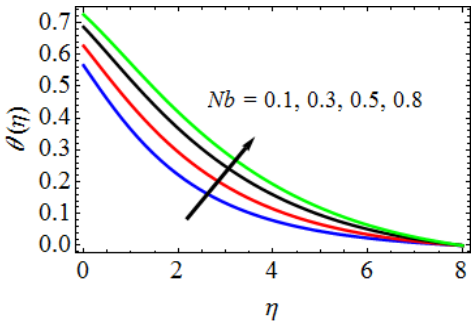

Fig. 10 *Temperature profiles for different values of Nb*

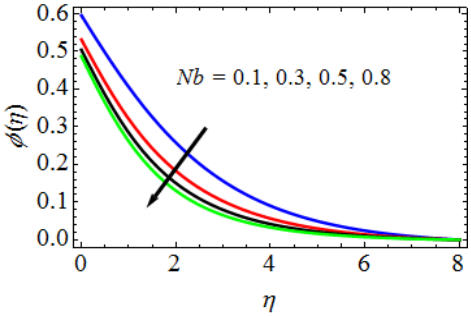

Fig. 11 *Concentration profiles for different values of Nb*

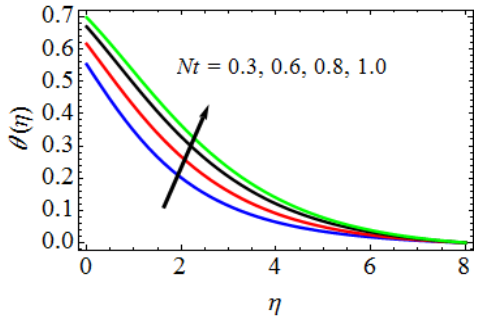

Fig. 12 *Temperature profiles for different values of Nt*

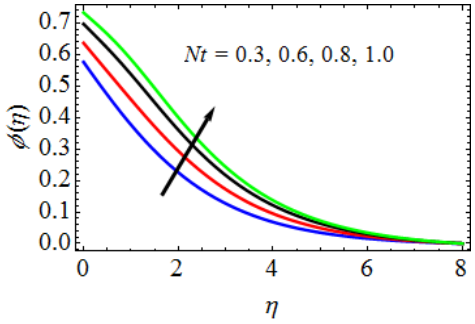

Fig. 13 *Concentration profiles for different values of Nt*

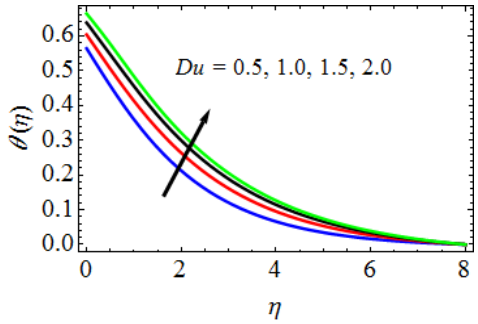

Fig. 14 *Temperature profiles for different values of Du*

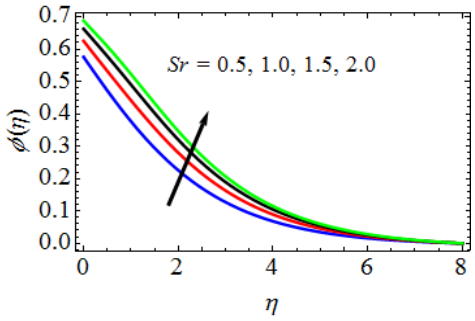

Fig. 15 *Concentration profiles for different values of Sr*

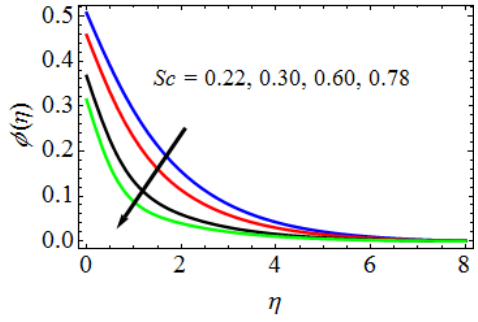

Fig. 16 *Concentration profiles for different values of Sc*

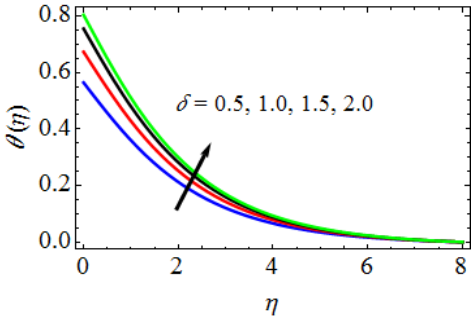

Fig. 17 *Temperature profiles for different values of δ*

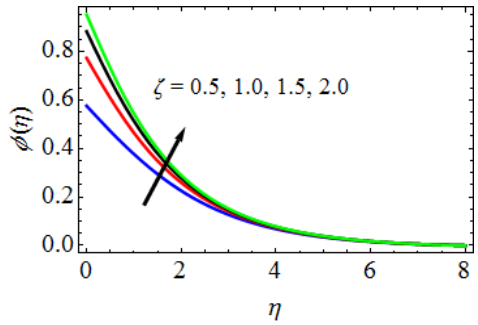

Fig. 18 *Concentration profiles for different values of ζ*

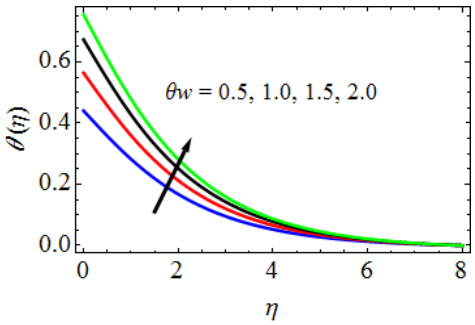

Fig. 19 *Temperature profiles for different values of θ_w*

Table 3 *Skin-friction coefficient along x-direction results*

M	K	C	Pr	R	Nb	Nt	Du	Sr	δ	θ_w	Sc	ζ	Cfx
0.5	0.5	0.5	0.71	0.5	0.1	0.3	0.5	0.5	0.5	0.5	0.22	0.5	2.546437343607360
1.0													2.508765263576013
1.5													2.485283485608439
	1.0												2.511653307016092
	1.5												2.498227960761376
		1.0											2.573626975708616
		1.5											2.597646669707338
			1.00										2.497668297702876
			3.00										2.471566153763403
				1.0									2.569875397576017
				1.5									2.581369967750863
					0.3								2.561586796734067
					0.5								2.595678294408389
						0.6							2.573556447687318
						0.8							2.606763778348901
							1.0						2.587897669879387
							1.5						2.611560653763762
								1.0					2.571640195387634
								1.5					2.597609707320919
									1.0				2.566763284374687
									1.5				2.586746385373134
										0.8			2.557680935490819
										1.0			2.569626675651756
											0.30		2.518692937410012
											0.78		2.491534986763187
												1.0	2.570688907763176
												1.5	2.591699835738061

Table 4 *Skin-friction coefficient along y-direction results*

M	K	C	Pr	R	Nb	Nt	Du	Sr	δ	θ_w	Sc	ζ	Cfy
0.5	0.5	0.5	0.71	0.5	0.1	0.3	0.5	0.5	0.5	0.5	0.22	0.5	1.876769736033409
1.0													1.846776160346039
1.5													1.829867876176030
	1.0												1.848767654776747
	1.5												1.815456987843870
		1.0											1.892867987198791
		1.5											1.916713760394867
			1.00										1.839257891257348
			3.00										1.817673676307610
				1.0									1.899867736837608
				1.5									1.914567650860163
					0.3								1.896673260987609
					0.5								1.912567187608761
						0.6							1.896572367177734
						0.8							1.911567318768012
							1.0						1.896786937865807
							1.5						1.910157087618845
								1.0					1.890867871769898
								1.5					1.919687613690091
									1.0				1.891606376097636
									1.5				1.917887637687018
										0.8			1.889867006317667
										1.0			1.900156738076087
											0.30		1.841676430761739
											0.78		1.829663409636473
												1.0	1.889365768772494
												1.5	1.899256010763901

Table 5 *Rate of heat transfer coefficient results*

Pr	*R*	*Nb*	*Nt*	*Du*	δ	θ_w	Nu_x
0.71	*0.5*	*0.1*	*0.3*	*0.5*	*0.5*	*0.5*	*1.596830981948893*
1.00							*1.540146983497358*
7.00							*1.522678298079871*
	1.0						*1.622579819879815*
	1.5						*1.640867673619807*
		0.3					*1.611567987134682*
		0.5					*1.632676708713469*
			0.6				*1.621674784390873*
			0.8				*1.643657036096307*
				1.0			*1.629676710760369*
				1.5			*1.646783093109616*
					1.0		*1.612669136036737*
					1.5		*1.633676846987895*
						1.0	*1.609561387560034*
						1.5	*1.620561387408763*

Table 6 *Rate of mass transfer coefficient results*

Nt	*Nb*	*Sc*	*Sr*	ζ	Sh_x
0.3	*0.1*	*0.22*	*0.5*	*0.5*	*1.865613746076340*
0.6					*1.899564701676437*
0.8					*1.921696347687664*
	0.3				*1.838673618736870*
	0.5				*1.810136763487613*
		0.30			*1.835639609613409*
		0.78			*1.817561348760834*
			1.0		*1.889365871387687*
			1.5		*1.909567613476763*
				1.0	*1.890563467630197*
				1.5	*1.915673413847891*

5. CONCLUSION

This work investigates the impact of Thermo-diffusion and Diffusion-thermo on a non-Newtonian Maxwell fluid with nanofluid particles, thermal and mass Biot numbers, Brownian motion, thermophoresis, and magnetic field. It models the problem using partial differential equations and numerically solves them, allowing visualization of velocity, temperature, and nanofluid concentration profiles. The conclusions of this study project are:

- ✓ Thermal radiation, thermophoresis, Brownian motion, Dufour number, thermal Biot number, and temperature ratio are all indicators of rising temperature profiles.
- ✓ The temperature profiles shrink as the Prandtl number increases.

- ✓ The concentration profiles get smaller as the magnitude of the Schmidt number, a Brownian motion parameter, rises.
- ✓ As the values of the Maxwell fluid and magnetic field parameters increase, the velocity profile in the x and y directions decreases, but the velocity ratio parameter has the opposite effect.
- ✓ The concentration profiles rise in tandem with the values of the Soret number, Mass Biot number, and thermophoresis parameter.
- ✓ Ultimately, under specific conditions, the present numerical findings match the published findings of [38] and [39] very well.

Applications

The present study addressed in this paper has several scientific and engineering applications, including the following:

- investigation of the interaction between a geomagnetic field and a geothermal location;
- petroleum engineering applications, involving the flow of oil, gas, and water via oil or gas reservoirs;
- blood flow analysis through arteries;
- soil mechanics, water purification, and powder metallurgy.

Nomenclature:

List of Symbols:

u, v, w : Velocity components in x, y and z Axes, respectively (m/s)

x, y, z : Cartesian coordinates measured along the stretching sheet (m)

f : Dimensionless stream function along the x - direction $(kg/m.s)$

f' : Fluid velocity along the x - direction(m/s)

g : Dimensionless stream function along the y - direction $(kg/m.s)$

g' : Fluid velocity along the y - direction(m/s)

Pr : Prandtl number

T : Fluid temperature (K)

T_f : Temperature of hot fluid (K)

T_∞ : Temperature of the fluid far away from the stretching sheet (K)

Cf_x : Skin-friction coefficient along x - direction (s^{-1})

Cfx : Non-dimensional skin-friction coefficient along x - direction (s^{-1})

M : Magnetic field parameter

B_o : Uniform magnetic field $(Tesla)$

a, b : Constants

T_w : Temperature at the surface (K)

O : Origin

Sc : Schmidt number

K : Maxwell fluid parameter

R : Thermal radiation parameter

q_r : Radiative heat flux

Cf_y : Skin-friction coefficient along y - direction (s^{-1})

Cfy : Non-dimensional Skin-friction coefficient along the y - direction (s^{-1})

$U_w(x)$: Stretching velocity of the fluid along the x - direction (m/s)

$V_w(y)$: Stretching velocity of the fluid along the y - direction (m/s)

q_w : Heat flux coefficient

q_m : Mass flux coefficient

Nt : Thermophoresis parameter

Nb : Brownian motion parameter

Nu : Rate of heat transfer coefficient (or) Nusselt number

Sh : Rate of mass transfer coefficient (or) Sherwood number

C_p : Specific heat capacity of nano particles ($J/kg/K$)

C : Stretching sheet parameter

Re_x : Reynolds number along the x - direction

Re_y : Reynolds number along the y - direction

D_B : Brownian diffusion coefficient (m^2/s)

D_T : Thermophoresis diffusion coefficient

Sr : Soret number

Du : Dufour number

K^* : Mean absorption coefficient

C_w : Dimensional nanoparticle volume Concentration at the stretching surface (mol/m^3)

C_∞ : Dimensional ambient volume fraction (mol/m^3)

C_s : Concentration susceptibility

K_T : Thermal diffusion ratio

D_m : Solutal diffusivity of the medium

T_m : Fluid Mean temperature

C_f : Dimensional Concentration of hot fluid (mol/m^3)

Greek symbols:

η : Dimensionless similarity variable (m)

θ : Dimensionless temperature (K)

ν : Kinematic viscosity (m^2/s)

σ : Electrical Conductivity

ρ : Fluid density (kg/m^3)

κ : Thermal conductivity of the fluid

τ_{wx} : Wall shear stress along the x - direction

τ_{wy} : Wall shear stress along the y - direction

ϕ : Dimensionless nano-fluid Concentration (mol/m^3)

δ : Thermal Biot number

ζ : Mass Biot number

β_1 : Non-uniform heat transfer coefficient

β_2 : Non-uniform mass transfer coefficient

α : Thermal diffusivity, (m^2/s)

θ_w : Temperature ratio parameter

φ : Fluid nanoparticle volume Concentration (mol/m^3)

φ_∞ : Dimensional ambient volume fraction (mol/m^3)

σ^* : Stefan-Boltzmann constant

λ : The fluid relaxation time

μ : Dynamic viscosity of the fluid

ρ_f : Density of the fluid (kg/m^3)

Superscript:

$'$: Differentiation w.r.t η

Subscripts:

f : Fluid

w : Condition on the sheet

∞ : Ambient Conditions

6. REFERENCES

[1] Chen, Y-J., Wang, P-Y., Liu, Z-H., Li, Y-Y., Heat transfer characteristics of a new type of copper wire-bonded flat heat pipe using nanofluids, *International Journal of Heat and Mass Transfer*, 67, 548-559, 2013. https://doi.org/10.1016/j.ijheatmasstransfer.2013.08.060

[2] Venkatesh, N., Raju, R.S., Anil Kumar, M., Dharmendar Reddy, Y., A numerical study on MHD Maxwell fluid with nanoparticles over a stretching surface: Impacts of thermal radiation, convective boundary condition and induced magnetic field, *Numerical Heat transfer, Part: Applications*, 1-16, 2024.

https://doi.org/10.1080/10407782.2024.2338259

[3] Madan Kumar, R., Srinivasa Raju, R., Kumar, M.A., Venkateswarlu, B., A numerical study of thermal and diffusion effects on MHD Jeffrey fluid flow over a porous stretching sheet with activation energy, *Numerical Heat Transfer, Part A: Applications*, 1–22, 2024.

https://doi.org/10.1080/10407782.2024.2319344

[4] Suhasini, R., Srinivasa Raju, R., Anil Kumar, M., Dharmendar Reddy, Y., Madan Kumar, R., A numerical study on MHD micropolar nanofluid flow over a Darcian porous stretching surface: impacts of thermophoretic and Brownian diffusions, *Radiation Effects and Defects in Solids*, 179(11–12), 1616–1631, 2024.

https://doi.org/10.1080/10420150.2024.2359679

[5] Rajakumar, K.V.B., Ranganath, N., Govinda Rao, T., Srinivasa Raju, R., Radiation absorption, Hall and ion-slip current – driven MHD convection with spanwise cosinusoidally fluctuating temperature: a perturbative study, *Radiation Effects and Defects in Solids*, 1–35, 2024. https://doi.org/10.1080/10420150.2024.2391775

[6] Mebarek-Oudina, F., Dharmaiah, G., Balamurugan, K.S., Ismail, A.I., Saxena, H., The Role of Quadratic-Linearly Radiating Heat Source with Carreau Nanofluid and Exponential Space-Dependent Past a Cone and a Wedge: A Medical Engineering Application and Renewable Energy, *Journal of Computational Biophysics and Chemistry*, 22(8), 997-1011 (2023).

https://doi.org/10.1142/S2737416523420073

[7] Dharmaiah, G., Mebarek-Oudina, F., Rama Prasad, J.L., Ch. Baby Rani, Exploration of Bio-convection for slippery two-phase Maxwell Nanofluid past a vertical induced magnetic stretching regime associated for Biotechnology and Engineering, *Journal of Molecular Liquids*, 391(8), 123408, 2023. https://doi.org/10.1016/j.molliq.2023.123408

[8] Ramesh, K., Mebarek-Oudina, F., Souayeh, B., *Mathematical Modelling of Fluid Dynamics and Nanofluids*, 1st edition, CRC Press (Taylor & Francis); 2023.

https://doi.org/10.1201/9781003299608

[9] Raza, J., Mebarek-Oudina, F., Ali, H., Sarris, I.E., Slip effects on Casson Nanofluid over a Stretching sheet with activation energy: RSM Analysis, *Frontiers in Heat and Mass Transfer*, 22(4), 1017-1041, 2024. https://doi.org/10.32604/fhmt.2024.052749

[10] Ould Said, B., Mabarek-Oudina, F., Medebber, M.A., Magneto-hydro-Convective Nanofluid flow in Porous Square Enclosure, *Frontiers in Heat and Mass Transfer*, 22(5), 1343-1360, 2024. https://doi.org/10.32604/fhmt.2024.054164

[11] Mezaache, A., Mebarek-Oudina, F., Vaidya, H., Ramesh, K., Impact of Nanofluids and Porous Structures on the Thermal Efficiency of Wavy Channel Heat Exchanger, *International Journal of Thermal Sciences*, 210, 109673, 2025.

https://doi.org/10.1016/j.ijthermalsci.2024.109673

[12] Xu, H.J., Qu, Z.G., Tao, W.Q., Analytical solution of forced convective heat transfer in tubes partially filled with metallic foam using the two-equation model, *International Journal of Heat and Mass Transfer*, 54(17-18), 3844-3850, 2011.

https://doi.org/10.1016/j.ijheatmasstransfer.2011.04.044

[13] Babu, N.V.N., Murali, G., Bhati, S.M., Casson fluid performance on natural convective dissipative couette flow past an infinite vertically inclined plate filled in porous medium with heat transfer, MHD and hall current effects, *International Journal of Pharmaceutical Research*, 10(4), 809-819, 2018.

http://www.ijpronline.com/ViewArticleDetail.aspx?ID=7303

[14] Deepa, G., Murali, G., Effects of viscous dissipation on unsteady MHD free convective flow with thermophoresis past a radiate inclined permeable plate, *Iranian Journal of Science and Technology, Transaction A* (Sciences), 38(A3), 379-388, 2014.

https://ijsts.shirazu.ac.ir/article_2437.html

[15] Deepa, G., Gundagani, M., Analysis of soret and dufour effects on unsteady MHD flow past a semi infinite vertical porous plate via finite difference method, *International Journal of Applied Physics and Mathematics*, 4(5), 332-344, 2014.

https://doi.org/10.7763/IJAPM.2014.V4.306

[16] Gundagani, M, Sheri, S., Paul, A., Reddy, M.C.K., Unsteady magnetohydrodynamic free convective flow past a vertical porous plate, *International Journal of Applied Science and Engineering*, 11 (3), 267–275, 2013. https://gigvvy.com/journals/ijase/articles/ijase-201309-11-3-267

[17] Kirubaharan, D.R., Subhashini, A.D., Murali, G., Study of Three Dimensional Casson-Nanofluid Flow due to a Linear Porous Stretching Sheet in the Presence of Double Diffusion Effects, *Advances in Systems Science and Applications*, 24(3), 90-103, 2024.

[18] Gundagani, M., Babu, N.V.N., GadPally, D., Bhati, S.M., Sanjay Ch, Nirmala Kasturi, V., Study of Nano-Powell-Erying fluid flow past a porous stretching sheet by the effects of MHD,

thermal and mass convective boundary conditions, *Journal of Umm Al-Qura University for Engineering and Architecture*, 15, 271-281, 2024.

https://doi.org/10.1007/s43995-024-00056-2

[19] Gundagani, M., Mamidi, L.P., Tanuku, P.K., Finite element solutions of Double diffusion effects on three-dimensional MHD Nano-Powell-Erying fluid flow in presence of thermal and mass Biot numbers, *Journal of Engineering and Applied Science*, 71, Article 9, 2024.

https://doi.org/10.1186/s44147-023-00347-w

[20] Murali, G., Paul, A., Babu, N.V.N., Heat and mass transfer effects on an unsteady hydromagnetic free convective flow over an infinite vertical plate embedded in a porous medium with heat absorption, *International Journal of Open Problems in Computer Science and Mathematics* (IJOPCM), 8 (1), 15-27, 2015. https://doi.org/10.12816/0010706

[21] Murali, G., Paul, A., Babu, N.V.N., Numerical study of chemical reaction effects on unsteady MHD fluid flow past an infinite vertical plate embedded in a porous medium with variable suction, *Electronic Journal of Mathematical Analysis and Applications* (EJMAA)*,* 3(2), 13, 179-192, 2015. https://doi.org/10.21608/ejmaa.2015.310762

[22] Murali, G., Deepa, G., Venkata Madhu, J., Nirmala Kasturi, V., Bhati, S.M., Narendra Babu, N., Three Dimensional Chemically Reacting Oldroyd-B Fluid + Nanofluid Flow in Presence of Thermophoresis and Brownian Motion Effects, *Discontinuity, Nonlinearity, and Complexity*, 14(2), 373-388, 2025. https://doi.org/10.5890/DNC.2025.06.010

[23] Murali, G., Deepa, G., Nirmala Kasturi, V., Poornakantha, T., Joint effects of thermal diffusion and diffusion thermo on MHD three dimensional nanofluid flow towards a stretching sheet, *Mathematical Models in Engineering*, 9(4), 130-143, 2023.

https://doi.org/10.21595/mme.2023.23590

[24] Murali, G., Babu, N.V.N., Convective MHD Jeffrey Fluid Flow Due to Vertical Plates with Pulsed Fluid Suction: A Numerical Study, *Journal of Computational Applied Mechanics*, 54 (1), 36-48, 2023. https://jcamech.ut.ac.ir/article_90604.html

[25] Reddy, M.K., Murali, G., Sivaiah, S., Babu, N.V.N., Heat and mass transfer effects on unsteady MHD free convection flow past a vertical permeable moving plate with radiation, *International Journal of Applied Mathematical Research*, 1(2), 189-205, 2012.

https://doi.org/10.14419/ijamr.v1i2.45

[26] Bhati, S.M., Murali, G., Sanjay, Ch., Law of elecric fields via bianchi identities, *Journal of Applied Science and Engineering*, 25(4), 759-762, 2022.

https://doi.org/10.6180/jase.202208_25(4).0011

[27] Sivaiah, S., Murali, G., Reddy, M.C.K., Finite Element Analysis of Chemical Reaction and Radiation Effects on Isothermal Vertical Oscillating Plate with Variable Mass Diffusion, *International Scholarly Research Network, ISRN Mathematical Physics*, Volume 2012, Article ID 401515, 2012. https://doi.org/10.5402/2012/401515

[28] Nagasmitha, B.R., Nagendramma, V., Ahmed, N., Marutamanikandan, S., Murali, G., Analytical Study of Nonlinear Behavior and Convection Patterns in Darcy-Brinkman Porous Medium with Maxwell-Cattaneo Ferroconvection, *Journal of Mines, Metals and Fuels*, 73(2), 437–445, 2025. https://doi.org/10.18311/jmmf/2025/47828

[29] Nagasmitha, B.R., Nagendramma, V., Ahmed, N., Marutamanikandan, S., Murali, G., Mathematical Modeling of Heat Transfer Phenomena in Darcy Porous Media with Couple-

Stress Magnetic Fluid under Maxwell-Cattaneo Model, Journal of Mines, Metals and Fuels, 73(2), 509–516, 2025. https://doi.org/10.18311/jmmf/2025/47825

[30] Sivaiah, S., Muraligoud, G., Murali, G., Reddy, M.C.K., Raju, S., Unsteady MHD mixed convection flow past a vertical porous plate in presence of radiation, *International Journal of Basic and Applied Sciences*, 1(4), 651-666, 2012.

https://doi.org/10.14419/ijbas.v1i4.106

[31] Tanuku, P.K., Mamidi, L.P., Gundagani, M., Modelling and analysis of three-dimensional chemically reacting, radiating Casson-nanofluid flow: thermophoresis and Brownian motion effects, *Acta Polytechnica*, 64(5), 455–463, 2024.

https://doi.org/10.14311/AP.2024.64.0455

[32] Shah, S.A.A., Ahammad, N.A., Din, E.M.T.E., Gamaoun, F., Awan, A.U., Ali, B., Bio-convection effects on Prandtl hybrid nanofluid flow with chemical reaction and motile microorganism over a stretching sheet, *Nanomaterials*, 12(13), 2174, 2022.

https://doi.org/10.3390/nano12132174

[33] Dharmaiah, G., Mebarek-Oudina, F., Balamurugan, K.S., Vedavathi, N., Numerical Analysis of the Magnetic Dipole Effect on a Radiative Ferromagnetic Liquid Flowing over a Porous Stretched Sheet, *Fluid Dynamics and Materials Processing*, 20(2), 293–310 (2024).

https://doi.org/10.32604/fdmp.2023.030325

[34] Mebarek-Oudina, F., Dharmaiah, G., Rama Prasad, J.L., Vaidya, H., Kumari, M.A., Thermal and Flow Dynamics of Magnetohydrodynamic Burgers' Fluid Induced by a Stretching Cylinder with Internal Heat Generation and Absorption, *International Journal of Thermofluids*, 25, 100986, 2025. https://doi.org/10.1016/j.ijft.2024.100986

[35] Anil Kumar, M., Mebarek-Oudina, F., Mangathai, P., Shah, N.A., Vijayabhaskar, Ch., Venkatesh, N., Fouad, Y., The Impact of Soret Dufour and Radiation on the Laminar Flow of a Rotating liquid past a Porous plate via Chemical Reaction, *Modern Physics Letters B*, 39(10), 2450458, 2025. https://doi.org/10.1142/S021798492450458X

[36] Fayz-Al-Asad, M., Mebarek-Oudina, F., Vaidya, H., Hasan, M.S., Sarker, M.M.A., Ismail, A.I., Finite Element Analysis for Magneto-convection Heat Transfer Performance in Vertical Wavy Surface Enclosure: Fin Size Impact, *Frontiers in Heat and Mass Transfer*, 22(3), 817-837, 2024. https://doi.org/10.32604/fhmt.2024.050814

[37] Ramasekhar, G., Mebarek-Oudina, F., Suneetha, S., Vaidya, H., Selvi, P.D., Computational simulation of Casson hybrid nanofluid flow with Rosseland approximation and uneven heat source/sink, International Journal of Thermofluids, 24, 100893, 2024.

https://doi.org/10.1016/j.ijft.2024.100893

[38] Mushtaq, A., Mustafa, M., Hayat, T., Alsaedi, A., A numerical study for three-dimensional viscoelastic flow inspired by non-linear radiative heat flux, *International Journal of Non-Linear Mechanics*, 79, 83-87, 2016. https://doi.org/10.1016/j.ijnonlinmec.2015.11.006

[39] Liu, I.C., Andersson, H.I., Heat transfer over a bidirectional stretching sheet with variable thermal conditions, *International Journal of Heat and Mass Transfer*, 51(15-16), 4018-4024, 2008. https://doi.org/10.1016/j.ijheatmasstransfer.2007.10.041